Baryon states with open beauty in the extended local hidden gauge approach

W. H. Liang,[1,2,*] C. W. Xiao,[2] and E. Oset[2]

[1]*Department of Physics, Guangxi Normal University, Guilin 541004, People's Republic of China*
[2]*Departamento de Física Teórica and IFIC, Centro Mixto Universidad de Valencia-CSIC,*
Institutos de Investigación de Paterna, Apartado 22085, 46071 Valencia, Spain

In this paper, we examine the interaction of $\bar{B}N$, $\bar{B}\Delta$, $\bar{B}^*N$, and $\bar{B}^*\Delta$ states, together with their coupled channels, by using a mapping from the light meson sector. The assumption that the heavy quarks act as spectators at the quark level automatically leads us to the results of the heavy quark spin symmetry for pion exchange and reproduces the results of the Weinberg Tomozawa term, coming from light vector exchanges in the extended local hidden gauge approach. With this dynamics we look for states dynamically generated from the interaction and find two states with nearly zero width, which we associate to the $\Lambda_b(5912)$ and $\Lambda_b(5920)$ states. The states couple mostly to $\bar{B}^*N$, which are degenerate with the Weinberg Tomozawa interaction. The difference of masses between these two states, with $J = 1/2$ and $3/2$, respectively, is due to pion exchange connecting these states to intermediate $\bar{B}N$ states. In addition to these two Λ_b states, we find three more states with $I = 0$, one of them nearly degenerate in two states of $J = 1/2$, $3/2$. Furthermore, we also find eight more states in $I = 1$, two of them degenerate in $J = 1/2$, $3/2$, and another two degenerate in $J = 1/2$, $3/2$, $5/2$.

I. INTRODUCTION

Hadron physics in the charm and beauty sectors is booming, with mounting activity in experiments *BABAR*, CLEO, BELLE, BES, LHC$_b$, and CDF [1–6] and theory [7]. One of the issues that has attracted much attention is the finding of hadronic states which cannot be interpreted in the conventional picture of $q\bar{q}$ for mesons and qqq for baryons. Multiquark states, hybrids, or hadronic molecules have been suggested in several works [8–18]. The molecular picture stands on firm grounds once the use of the chiral unitary theory in the light quark sector, or its extension through the local hidden gauge approach, has shown that many mesonic and baryonic resonances are dynamically generated from the interaction of more elementary hadron components [19,20]. Concerning baryonic resonances with charm or hidden charm, work on molecules has been done in Refs. [21–29], while, in the beauty sector, baryon states with beauty or hidden beauty have also been studied in Refs. [30–33].

On the experimental side, Λ_b excited states have been reported by the LHC$_b$ Collaboration in Ref. [34]. Two states, $\Lambda_b(5912)$ and $\Lambda_b(5920)$, are found in the experiment, with widths smaller than 0.66 MeV in both cases. Although no direct spin and parity have been determined, the states are interpreted as orbitally excited states of the ground state of the $\Lambda_b(5619)$. One of the states, the $\Lambda_b(5920)$, has been confirmed by the CDF Collaboration in Refs. [35,36]. The association to the orbitally excited states

of the $\Lambda_b(5619)$ seems most natural, since predictions of quark models had been done for these states, as the orbitally excited Λ_b states with $L = 1$ and $J^P = 1/2^-$, $3/2^-$ [37,38]. Compared to the observed results, the Λ_b masses, including that of the ground state, are only off by about 30–35 MeV.

The closest work in spirit to the present one is that of Ref. [31], where these states are dynamically generated from the interaction of mesons and baryons. In Ref. [31], the heavy quark spin symmetry (HQSS) is used as an underlying symmetry. According to it, the B and B^* states are degenerate in the heavy quark limit, as well as the $J^P = 1/2^+$, $3/2^+$ baryon states, which are then considered together in a coupled channels approach. An extrapolation of the Weinberg Tomozawa interaction in the light sector is then used [28,31], with elements of an SU(6) spin-isospin symmetry [39]. With suitable choices of the renormalization scheme for the loops, good agreement with the masses of the newly found Λ_b states is obtained. Our scheme takes advantage of the study done in Refs. [29,32,40]. In those works, it was found that the use of the extended local hidden gauge approach to the heavy quark sector fully respects the HQSS, but it provided a dynamics different from the one of Ref. [31]. In particular, the connection between B and B^* states (or baryon states with $J^P = 1/2^+$, $3/2^+$) requires pion exchange, or anomalous terms, which are found to be subleading in the large heavy quark mass counting and numerically small. Similar conclusions are also found in Ref. [41]. In some works [42], pion exchange is found to be relevant compared to vector meson exchange (the dominant terms in the local hidden gauge approach), but, as discussed in Ref. [40], this is in part due to the use of

*liangwh@gxnu.edu.cn

a type of form factor for vector mesons, not present when the equivalent chiral amplitudes are constructed, that suppresses the vector exchange.

With the dynamics of the extended local hidden gauge approach, the number of coupled channels is small for each quantum number, and we can get a good feeling of the basic building blocks in the dynamically generated states that appear. As we shall see, the two Λ_b excited states are generated with masses close to the experimental ones, but, more remarkable, the difference in the masses of the two excited states agrees well with experiment. The widths obtained are zero within our basis of coupled channels, quite in agreement with the widths smaller than 0.66 MeV found in the experiment. We also make predictions in other isospin and spin sectors. On the formal aspects we show how the dominant terms correspond to having a heavy quark as a spectator and present an easy way to implement the results of the heavy quark spin-flavor symmetry from the impulse approximation at the quark level.

II. FORMALISM

We will look at the states $\pi\Sigma_b$, $\pi\Lambda_b$, $\eta\Lambda_b$, $\eta\Sigma_b$, and $\bar{B}N$ which can couple to $I = 0$, 1which we will investigate. Similarly, we shall look at $\bar{B}^*N$ and $\pi\Sigma_b^*$, $\eta\Sigma_b^*$, $\bar{B}\Delta$, and $\bar{B}^*\Delta$, with $\Delta \equiv \Delta(1232)$ and $\Sigma_b^* = \Sigma_b^*(5829)$, belonging to a decuplet of $3/2^+$ states. In the local hidden gauge approach in SU(3) [43–45], the meson-baryon interaction proceeds via the exchange of vector mesons as depicted in Fig. 1. As discussed in Ref. [29], when we exchange a light vector meson in Figs. 1(a) and 1(b), the heavy quarks of the meson or the baryon are spectators, and hence the interaction does not depend on their spin nor its flavor. From the technical point of view, the interaction of the diagrams of Fig. 1 can be obtained by using SU(3) symmetry considering u, d, b quarks, since we do not consider states with strangeness or hidden strangeness. Thus, all matrix elements of the interaction are formally identical (except for the mass or energy dependence) to those found for the interaction of the analogous states $\pi\Sigma$, $\pi\Lambda$, $\eta\Lambda$, $\eta\Sigma$, $\bar{K}N$, $\bar{K}^*N$, $\pi\Sigma^*$, $\eta\Sigma^*$, $\bar{K}\Delta$, and $\bar{K}^*\Delta$. This interaction has been studied in Refs. [46,47].

The transition potential from channel i to channel j is given by [48]

$$V = -C_{ij}\frac{1}{4f^2}(2\sqrt{s} - M_{B_i} - M_{B_j})\sqrt{\frac{M_{B_i} + E_i}{2M_{B_i}}}\sqrt{\frac{M_{B_j} + E_j}{2M_{B_j}}},$$

(1)

with f the pion decay constant and M_{B_i} and E_i (M_{B_j} and E_j) the mass and energy, respectively, of the baryon of the i (j) channel. We take $f = f_\pi = 93$ MeV, since we exchange light vector mesons. The C_{ij} coefficients are evaluated in Refs. [46,47], and we quote them below.

For pseudoscalar mesons and $1/2^+$ baryons, we have the coupled channels $\bar{B}N$, $\pi\Sigma_b$, and $\eta\Lambda_b$ in $I = 0$, and the C_{ij} coefficients are given in Table I. In $I = 1$, we have the channels $\bar{B}N$, $\pi\Sigma_b$, $\pi\Lambda_b$, and $\eta\Sigma_b$, and the C_{ij} coefficients are given in Table II. As one can see, the interaction in $I = 0$ is stronger than that in $I = 1$, and we have more chances to bind states in $I = 0$.

As discussed in Ref. [29], the mixing of states containing baryons of the octet (in u, d, b) like Σ_b and of the decuplet Σ_b^* require pion exchange for their mixing, and this is strongly suppressed in the heavy quark sector; hence, we neglect the mixing in a first step, but we shall come back to it in Sec. V. Then, if we consider a pseudoscalar meson and a baryon of the decuplet, we have the results for C_{ij} given in Tables III and IV [47]. We note that the strength of the $\bar{B}\Delta \to \bar{B}\Delta$ coefficient is 4 times bigger than for $\bar{B}N \to \bar{B}N$ and, thus, we expect larger bindings in this case.

The interaction $\bar{B}\Delta$ and coupled channels with $I = 2$ is repulsive, and we do not consider it.

In coupled channels we will use the Bethe-Salpeter equation

$$T = [1 - VG]^{-1}V,$$

(2)

with G the diagonal loop function for the propagating intermediate meson-baryon channels. In Ref. [32], we warned about potential dangers of using the dimensional regularization for the G functions (see also Ref. [30]), since for values of the energy below threshold G can soon become positive, and then one can be misled to obtain bound states with a positive (repulsive) potential when $1 - VG = 0$ [see Eq. (2) in one channel]. For this reason, we also use here the cutoff regularization for G given by
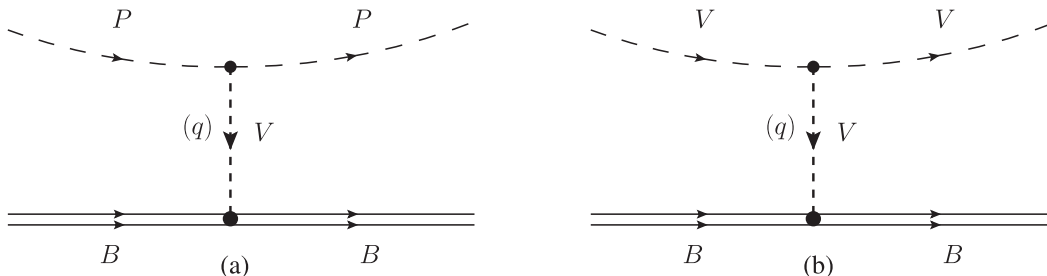

FIG. 1.   Diagrammatic representation of the pseudoscalar-baryon interaction (a) and vector-baryon interaction (b).

TABLE I. C_{ij} coefficients for $\bar{B}N$ and coupled channels with $I = 0$ and $J^P = 1/2^-$.

C_{ij}	$\bar{B}N$	$\pi\Sigma_b$	$\eta\Lambda_b$
$\bar{B}N$	3	$-\sqrt{\frac{3}{2}}$	$\frac{3}{\sqrt{2}}$
$\pi\Sigma_b$		4	0
$\eta\Lambda_b$			0

TABLE II. C_{ij} coefficients for $\bar{B}N$ and coupled channels with $I = 1$ and $J^P = 1/2^-$.

C_{ij}	$\bar{B}N$	$\pi\Sigma_b$	$\pi\Lambda_b$	$\eta\Sigma_b$
$\bar{B}N$	1	-1	$-\sqrt{\frac{3}{2}}$	$-\sqrt{\frac{3}{2}}$
$\pi\Sigma_b$		2	0	0
$\pi\Lambda_b$			0	0
$\eta\Sigma_b$				0

TABLE III. C_{ij} coefficient for $\pi\Sigma_b^*$ with $I = 0$ and $J^P = 3/2^-$.

C_{ij}	$\pi\Sigma_b^*$
$\pi\Sigma_b^*$	4

TABLE IV. C_{ij} coefficients for $\bar{B}\Delta$ and coupled channels with $I = 1$ and $J^P = 3/2^-$.

C_{ij}	$\bar{B}\Delta$	$\pi\Sigma_b^*$	$\eta\Sigma_b^*$
$\bar{B}\Delta$	4	1	$\sqrt{6}$
$\pi\Sigma_b^*$		2	0
$\eta\Sigma_b^*$			0

$$G(s) = \int_0^{q_{max}} \frac{d^3\vec{q}}{(2\pi)^3} \frac{\omega_P + \omega_B}{2\omega_P\omega_B} \frac{2M_B}{P^{02} - (\omega_P + \omega_B)^2 + i\varepsilon},$$

(3)

where $\omega_P = \sqrt{\vec{q}^2 + m_P^2}$, $\omega_B = \sqrt{\vec{q}^2 + M_B^2}$, and q_{max} is the cutoff of the three-momentum. However, in Ref. [32], we also took into account the form factor from vector meson exchange, by introducing

$$f(\vec{q}) = \frac{m_V^2}{\vec{q}^2 + m_V^2},$$

(4)

in which case we would have to replace Eq. (3) by

$$G(s) = \int \frac{d^3\vec{q}}{(2\pi)^3} f(\vec{q}) \frac{\omega_P + \omega_B}{2\omega_P\omega_B} \frac{2M_B}{P^{02} - (\omega_P + \omega_B)^2 + i\varepsilon},$$

(5)

putting the extra $f(\vec{q})$ factor. We would like to make a comment here, since in Ref. [32] we put $f^2(\vec{q})$. From the

practical point of view, the differences between the two choices are smaller than uncertainties we will accept from other sources. From the theoretical point of view, while the first loop implicit in Eq. (2), VGV, contains $f^2(\vec{q})$, the terms in the series go as VGV, $VGVGV$, $VGVGVGV$, …, and the ratio of one term to the other is GV. Hence, it is more appropriate to take just the one form factor of the potential V and include it in the G function when integrating over $\vec{q}$.

Since the G function in Eq. (3) is logarithmically divergent, the inclusion of $f(\vec{q})$ in Eq. (5) makes it already convergent. Yet we will put an extra cutoff q_{max} that will serve to fine-tune our T matrix and the binding of the states. We shall fine-tune q_{max} in the integral of Eq. (3), and we shall need values q_{max} smaller than $M_V \approx 780$ MeV. Hence, from the practical point of view, we can even neglect the factor $f(\vec{q})$ and effectively include its effects with the use of a suited value of q_{max}.

Before closing this section, we must say two words concerning the transition $\pi\Sigma_b \to \bar{B}N$. This is depicted in Fig. 2, and it is mediated by B^* exchange in the extended local hidden gauge approach. In the strict large heavy quark mass, counting this term would be neglected, because it involves the exchange of a heavy vector B^* and its propagator would render this term negligible. However, although suppressed, it is not so much as one would expect. Indeed, the propagator will be

$$D_{B^*} = \frac{1}{p_{B^*}^2 - m_{B^*}^2} \equiv \frac{1}{(p_\pi^0 - p_{\bar{B}}^0)^2 - (\vec{p}_\pi - \vec{p}_{\bar{B}})^2 - m_{B^*}^2}.$$
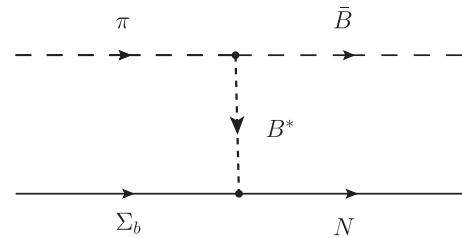
(6)

By contrast, in a diagonal transition $\bar{B}N \to \bar{B}N$ mediated by ρ exchange, for instance, we would have

$$D_\rho \approx \frac{1}{m_V^2}.$$

(7)

Close to the $\bar{B}N$ threshold, the ratio is

$$\frac{D_{B^*}}{D_\rho} \simeq \frac{m_V^2}{(p_\pi^0 - p_{\bar{B}}^0)^2 - \vec{p}_\pi^2 - m_{B^*}^2} \simeq \frac{1}{4}.$$

(8)

Since the nondiagonal terms have a smaller importance in the process than the diagonal ones of the heavy mesons, we

FIG. 2. Transition potential from $\pi\Sigma_b \to \bar{B}N$.

simply account for these transitions by multiplying by 1/4 the results obtained from Eq. (1) and the tables.

III. RESULTS FOR $I = 0$

We first choose the single channel $\pi\Sigma_b^*$ in $I = 0$ and look for the binding energy. The state with $L = 0$ has $J = 3/2$. First we find that with the normal potential and a wide range of cutoffs (up to 3000 MeV) we do not find a bound state. We must look at the reason for this in the fact that the potential is indeed weak. This is so because the potential in Eq. (1) is a relativistic form of $k^0 + k'^0$ (the sum of the incoming and outgoing pion energies). The small mass of the π makes its energy small close to threshold, and this potential is subleading with respect to the one of $\bar{B}N$ where the energies now are those of the $\bar{B}$.

Next we try to see if by increasing the potential by a factor of 1.5 or 2 and varying the cutoff we can obtain a reasonable binding. The results are chosen in Table V. As we can see, we have to increase the potential by a factor of 2 and go to very large cutoffs to obtain the desired value of the binding of the $\Lambda_b(5920)$. We might think that an increase by about a factor of 1.5 of the potential could be accepted by recalling that such changes appear in models like the Dyson-Schwinger approach [49] (see also Ref. [29]). Indeed, with respect to the coupling we would be using here, the $D\rho D$ coupling used in Ref. [49], or in Ref. [50] obtained with sum rules, is about a factor of 1.5 bigger. However, in the same work of Ref. [49], the coupling is accompanied by a form factor which would be equivalent to a cutoff q_{max} of about 700 MeV. Hence, we cannot invoke simultaneously an increase of the potential by a factor of 2 and a q_{max} of 3000 MeV, and the only conclusion is that the $\pi\Sigma_b^*$ channel by itself cannot account for the $\Lambda_b(5920)$ state.

Next we repeat the same exercise with the single channel $\bar{B}N$ and show the results in Table VI. What we see in this table is that the binding grows spectacularly (and

unrealistically) for bigger V and q_{max}. Obviously, the large value of the potential, as we mentioned above, is responsible for this. At this point, we should mention that in the study of the $\bar{K}N$ system in coupled channels a cutoff of 630 MeV was used in Ref. [46]. In the study of the pseudoscalar mesons with the decuplet of baryons [47], a value of $q_{max} = 700$ MeV was used, while in Ref. [30] in the study of baryons with hidden beauty a value of $q_{max} = 800$ MeV was used. We can also see in Table V that changes in V can be accommodated by a change in q_{max}. In what follows, we shall then use the potential that we get in the approach, without the extra multiplicative factor, but play with values of q_{max} around 700–850 MeV, in the range of values used in previous works.

In most of the cases, we get energies where all the coupled channels are closed and, hence, the width is zero. When there are open channels, we look for poles in the second Riemann sheet, which is obtained by changing the G function as [51]

$$G_l^{II}(\sqrt{s}) = G_l^{I}(\sqrt{s}) + i\frac{q_l}{4\pi\sqrt{s}}, \qquad (9)$$

where q_l is the on-shell momentum of the particles in the open channel and $G_l^{I}(\sqrt{s})$ is given by Eq. (3).

As an example, we show next the results without a form factor of Eq. (4) for $\bar{B}N$, just changing q_{max}, as shown in Table VII.

Next we introduce the coupled channels that couple to $\bar{B}N$ in $I = 0$ (see Table I). The results that we obtained for the energy are shown in Table VIII.

The results are interesting. We see now that we get two states rather than one. In order to get a feeling of the meaning of the states, we calculate the coupling of those states to the different coupled channels. We show the results in Table IX for $q_{max} = 800$ MeV. We show the values of the couplings (g_i^2 is the residue of the matrix element T_{ii} at the pole) and of $g_i G_i^{II}$, which, according to Ref. [52], provides the wave function of the origin in coordinate space, the magnitude that shows the relevance of the channel in the short-range strong interactions. It is interesting to see that there has been an appreciable mixture of these channels. The lower-energy state that originally was formed from $\bar{B}N$ alone now is still dominated by the $\bar{B}N$ channel but with an appreciable mixture of $\pi\Sigma_b$ and $\eta\Lambda_b$. On the other hand, the higher-energy state is shown to be dominated by the $\pi\Sigma_b$ channel. However, the coupling to the $\bar{B}N$ state has been essential to obtain this state, since the single channel $\pi\Sigma_b$ does not produce it.

TABLE V. Energies for the $\pi\Sigma_b^*$-only channel as a function of V and q_{max} (unit, MeV).

q_{max}	800	1000	1200	1400	1600	1800	2000	3000
$1.5V$	5971	5965	5961	5956	5953	5950	5948	5942
$2V$	5955	5947	5940	5935	5932	5929	5927	5920

TABLE VI. Energies for the $\bar{B}N$-only channel as a function of V and q_{max} (unit, MeV).

q_{max}	700	800	1000	1200	1400	1600	1800	2000
$1V$	6074	6026	5933	5851	5782	5725	5678	5639
$1.5V$	5967	5896	5766	5658	5572	5504	5450	5406
$2V$	5871	5784	5630	5509	5415	5343	5287	5243

TABLE VII. Energies for a state of $\bar{B}N$ in $I = 0$ as a function of q_{max} (unit, MeV).

q_{max}	700	750	800	850
V	5987.5	5941.6	5893.5	5843.7

TABLE VIII. Energies for states in coupled channels $\bar{B}N$, $\pi\Sigma_b$, and $\eta\Lambda_b$ in $I = 0$ as a function of q_{max} (unit, MeV).

q_{max}	700	750	800	850
V	5935.3	5897.3	5851.4	5802.0
	$6005.8 + i23.8$	$5988.9 + i26.4$	$5976.9 + i24.4$	$5968.0 + i20.5$

If one compares the energy of the lower-energy state in Table VIII with that of the single $\bar{B}N$ channel in Table VII, we can see that for $q_{max} = 800$ MeV the effect of the coupled channels has been a reduction of about 40 MeV. Hence, even if suppressed, the coupled channels to the $\bar{B}N$ have a relevant role in the generation of states. In any case, we see that neither of the states found can qualify as the $\Lambda_b(5912)$ or $\Lambda_b(5920)$. This is also the case for the higher-energy state.

After this, we exploit another possibility, that these Λ_b states come from $\bar{B}^*N$ and coupled channels. The $\bar{B}^*N$ can lead to two spins, $J^P = 1/2^-$, $3/2^-$, and within the local hidden gauge approach the interaction is spin independent [53]. Then we would get two degenerate states with spins 1/2 and 3/2. The 8 MeV difference between $\Lambda_b(5912)$ and $\Lambda_b(5920)$ is small enough to fit into the category of degenerate. The degeneracy is broken with the mixture of the VB and PB states, which is done in Refs. [54–56], but for the heavier mesons this mixture is smaller [29], which can explain the small difference between the masses of the two states. We shall come back to this point in the next two sections.

The binding of $\bar{B}N$ in Table VII for $q_{max} \sim$ 750–800 MeV is of the order of 300 MeV. While this is only 5% of the total energy, it might surprise us that this amount is about 3 times bigger than the one obtained in Refs. [30,32] for hidden beauty baryons ($B\Sigma_b$ is the equivalent component), but this is easy to understand, both qualitatively and quantitatively. Indeed, in the exchange of light vectors between $\bar{B}$ and N, the nucleon has three light quarks, while in the exchange of a light vector between B and Σ_b, the Σ_b has only two light quarks. There are, hence, more chances to exchange a light vector between $\bar{B}N$ than in $B\Sigma_b$. More quantitatively, if we take $I = 0$ for $\bar{B}N$, we have two components: $\bar{B}^0(b\bar{d})n(udd)$ and $\bar{B}^-(b\bar{u})p(uud)$.

We have two d quarks from the n to accommodate the exchange of a light $q\bar{q}$ in the first component and two u quarks in the second component. If we take $B\Sigma_b$ in $I = 1/2$, which was found bound in Ref. [32], we have the components $B^0(\bar{b}d)\Sigma_b^+(uub)$ and $B^+(\bar{b}u)\Sigma_b^0(udb)$. In the first case we cannot exchange a light $q\bar{q}$ vector, and in the second case there is only one u quark in the Σ_b^0 that can accommodate it. The strength of light vector exchange in $\bar{B}N$, $I = 0$, should be much larger than in $B\Sigma_b$, $I = 1/2$. This is the case in practice, since, comparing Table I of the present paper with Eqs. (2) and (12) of Ref. [32], we find that the relevant C_{ij} coefficient is 3 for $\bar{B}N$ and 1 for $B\Sigma_b$. As a consequence, we have the about 3 times larger binding found here with respect to the one of Refs. [30,32].

IV. VECTOR-BARYON CHANNELS

The transitions $VB \to VB$ for small momenta of the vector mesons have formally the same expressions as the corresponding $PB \to PB$ substituting the octet of pseudoscalars by the octet of vectors [53], with only one minor change to account for the ϕ and ω SU(3) structure, which is to replace each η by $-\sqrt{2/3}\phi$ or $\sqrt{1/3}\omega$. The case of vector interaction with the decuplet of baryons is similar [57]. Tables I, II, and IV are changed now to Tables X, XI,

TABLE X. C_{ij} coefficients for $\bar{B}^*N$ and coupled channels for $I = 0$ and $J^P = 1/2^-$, $3/2^-$.

C_{ij}	$\bar{B}^*N$	$\rho\Sigma_b$	$\omega\Lambda_b$	$\phi\Lambda_b$
$\bar{B}^*N$	3	$-\sqrt{\frac{3}{2}}$	$\sqrt{\frac{3}{2}}$	$-\sqrt{3}$
$\rho\Sigma_b$		4	0	0
$\omega\Lambda_b$			0	0
$\phi\Lambda_b$				0

TABLE IX. The coupling constants to various channels for certain poles in the $J = 1/2$, $I = 0$ sector.

$5851.4 + i0$	$\bar{B}N$	$\pi\Sigma_b$	$\eta\Lambda_b$
g_i	16.20	0.96	1.47
$g_i G_i^{II}$	-20.55	-16.23	-14.31

$5976.9 + i24.4$	$\bar{B}N$	$\pi\Sigma_b$	$\eta\Lambda_b$
g_i	$5.88 - i0.24$	$1.52 + i0.75$	$0.75 + i0.02$
$g_i G_i^{II}$	$-9.60 - i0.16$	$-53.13 - i12.34$	$-9.33 - i0.85$

TABLE XI. C_{ij} coefficients for $\bar{B}^*N$ and coupled channels for $I = 1$ and $J^P = 1/2^-$, $3/2^-$.

C_{ij}	$\bar{B}^*N$	$\rho\Sigma_b$	$\rho\Lambda_b$	$\omega\Sigma_b$	$\phi\Sigma_b$
$\bar{B}^*N$	1	-1	$-\sqrt{\frac{3}{2}}$	$-\sqrt{\frac{1}{2}}$	1
$\rho\Sigma_b$		2	0	0	0
$\rho\Lambda_b$			0	0	0
$\omega\Sigma_b$				0	0
$\phi\Sigma_b$					0

TABLE XII. C_{ij} coefficients for $\bar{B}^*\Delta$ and coupled channels for $I = 1$ and $J^P = 1/2^-, 3/2^-, 5/2^-$.

C_{ij}	$\bar{B}^*\Delta$	$\rho\Sigma_b^*$	$\omega\Sigma_b^*$	$\phi\Sigma_b^*$
$\bar{B}^*\Delta$	4	1	$\sqrt{2}$	-2
$\rho\Sigma_b^*$		2	0	0
$\omega\Sigma_b^*$			0	0
$\phi\Sigma_b^*$				0

and XII, respectively. Once again, we penalize with a factor of 1/4 the transitions from a heavy vector to a light vector as we did before for the pseudoscalar mesons.

We take again the case of $I = 0$ of Table X and show the results that are obtained in Table XIII for a $\bar{B}^*N$ single channel and in Table XIV for coupled channels. Once again, we see that the consideration of coupled channels leads to two states. In order to see the meaning of the states, we calculate again the couplings to the different channels for $q_{max} = 800$ MeV, and the results are shown in Table XV. There we can see that the state that couples strongly to $\bar{B}^*N$ is the one with lower energy. The higher-energy state couples mostly to $\rho\Sigma_b$.

It is interesting to compare the results of Tables VII and XIII for the states that couple mostly to $\bar{B}N$ and $\bar{B}^*N$. If we calculate with a single channel, we find a difference in energies between these two levels of 45 MeV, the same as between m_{B^*} and m_B. However, when we include the

TABLE XIII.   Energies for a state of $\bar{B}^*N$ in $I = 0$ as a function of q_{max} (unit, MeV).

q_{max}	700	750	800	850
V	6033.1	5987.2	5939.0	5889.3

TABLE XIV.   Energies for states in coupled channels $\bar{B}^*N$, $\rho\Sigma_b$, $\omega\Lambda_b$, and $\phi\Lambda_b$ in $I = 0$ as a function of q_{max} (unit, MeV).

q_{max}	700	750	800	850
V	6019.2	5970.6	5919.8	5867.6
	$6364.6 + i0.8$	$6333.3 + i0.8$	$6303.0 + i0.6$	$6274.1 + i0.3$

coupled channels, we see some changes. If we compare Tables XIII and XIV at $q_{max} = 800$ MeV, the effect of the coupled channels is a reduction of the mass of the lower state by about 20 MeV rather than 40 MeV in the case of $\bar{B}N$. The difference in the masses of the $\pi\Sigma_b$ or $\rho\Sigma_b$ is one of the reasons for it, but also the interaction of these two channels is different. Indeed, the VVV vertices or PPV vertices go as the sum of the external energies, as we saw, but now we have the much larger energy of the ρ instead of the energy of the π.

V. BREAKING THE $J = 1/2^-$, $3/2^-$ DEGENERACY IN THE $\bar{B}^*N$ SECTOR

In this section, we shall break the degeneracy of the $1/2^-$, $3/2^-$ states of the $\bar{B}^*N$ sector. For this purpose, we follow the approach of Ref. [54] and mix states of $\bar{B}^*N$ and $\bar{B}N$ in both sectors. We test first that, in the coupled channels like the $\bar{B}^*N$ sector, the important contribution comes from $\bar{B}^*N \to X \to \bar{B}^*N$, where X stands for the other coupled channels. The extra interaction of the X channels among themselves is negligible compared to that of the dominant $\bar{B}^*N$ channel because of the big value of the $\bar{B}^*$ energy entering in the interaction. This means that it is sufficient to evaluate the contribution of the box diagrams of Fig. 3, in analogy to the box diagrams evaluated in Ref. [54], and add this contribution δV to the $\bar{B}N$ or $\bar{B}^*N$ potential. By using the doublets of isospin (B^+, B^0), $(\bar{B}^0, -B^-)$, the Λ_b state in the $\bar{B}N$ basis is given by

$$|\bar{B}N, I = 0\rangle = \frac{1}{\sqrt{2}}(|\bar{B}^0n\rangle + |B^-p\rangle), \qquad (10)$$

and analogously for $\bar{B}^*N$. The $\bar{B}N \to \bar{B}^*N$ transition in $I = 0$ is given by the diagrams in Fig. 4.

The $VP\pi$ vertex in SU(3) is given by the Lagrangian

$$\mathcal{L}_{VPP} = -ig\langle[P, \partial_\mu P]V^\mu\rangle, \qquad (11)$$

where P and V^μ are the ordinary meson octet and vector nonet SU(3) matrix, respectively, of the corresponding fields

TABLE XV.   The coupling constants to various channels for certain poles in the $J = 1/2, 3/2, I = 0$ sector.

$5919.8 + i0$	$\bar{B}^*N$	$\rho\Sigma_b$	$\omega\Lambda_b$	$\phi\Lambda_b$
g_i	16.81	1.04	0.94	1.33
$g_i G_i^{II}$	-22.01	-5.46	-6.16	-5.67

$6303.0 + i0.6$	$\bar{B}^*N$	$\rho\Sigma_b$	$\omega\Lambda_b$	$\phi\Lambda_b$
g_i	$0.37 + i0.27$	$5.14 + i0.01$	$0.15 + i0.01$	$0.21 + i0.02$
$g_i G_i^{II}$	$-2.73 - i0.27$	$-46.81 - i0.13$	$-2.22 - i0.22$	$-1.50 - i0.15$
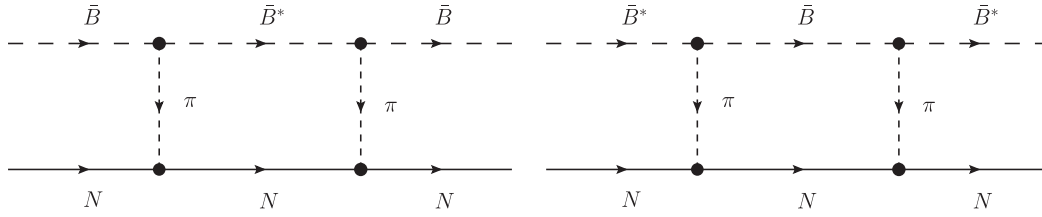
FIG. 3.   Diagrammatic representation of the $\bar{B}^*N$ in the intermediate state (left) and the $\bar{B}N$ in the intermediate state (right).
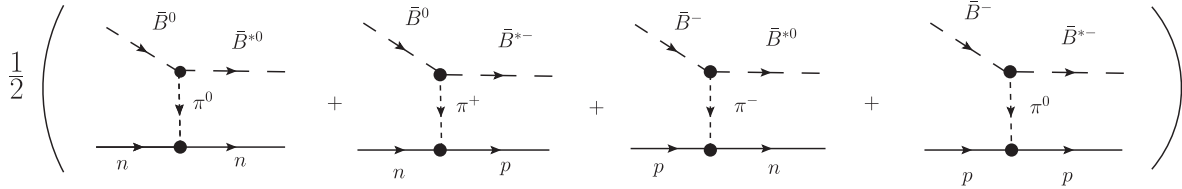
FIG. 4.   Diagrammatic representation of the transition $\bar{B}N \to \bar{B}^*N$ in $I = 0$.

$$P = \begin{pmatrix} \frac{\pi^0}{\sqrt{2}} + \frac{\eta_8}{\sqrt{6}} & \pi^+ & K^+ \\ \pi^- & -\frac{\pi^0}{\sqrt{2}} + \frac{\eta_8}{\sqrt{6}} & K^0 \\ K^- & \bar{K}^0 & -\frac{2\eta_8}{\sqrt{6}} \end{pmatrix}, \qquad (12)$$

$$V_\mu = \begin{pmatrix} \frac{\rho^0}{\sqrt{2}} + \frac{\omega}{\sqrt{2}} & \rho^+ & K^{*+} \\ \rho^- & -\frac{\rho^0}{\sqrt{2}} + \frac{\omega}{\sqrt{2}} & K^{*0} \\ K^{*-} & \bar{K}^{*0} & \phi \end{pmatrix}_\mu, \qquad (13)$$

and $g = m_V/2f_\pi$ with $m_V \approx 780$ MeV, $f_\pi = 93$ MeV. One can extend the Lagrangian Eq. (11) to the SU(4) space, as done in Ref. [40], but it is unnecessary. It is more intuitive and rigorous to follow the derivation below, which allows us to directly connect with the results of heavy quark spin-flavor symmetry [58]. Indeed, all we need to do is to invoke that the leading terms correspond to light meson exchange, in which case the heavy quark plays the role of a spectator at the quark level.

Let us then compare the $K^{*+} \to K^0\pi^+$ and $B^{*+} \to B^0\pi^+$ transitions as shown in Fig. 5. As we can see in the figure, the transitions are identical and governed by the light quarks, with the $\bar{s}$ quark in K^{*+} and $\bar{b}$ quark in B^{*+} playing the role of a spectator. The transition amplitudes are thus identical at the quark microscopic level, but we must take into account that when used at the macroscopic level of the K^{*+} or B^{*+} there are normalization factors $(2\omega)^{-1/2}$ which are different for the K^{*+}, K^0 or B^{*+}, B^0 fields. This is taken easily into account by constructing the S matrix at the macroscopic level. At the microscopic level we have (we follow Mandl + Shaw normalization of the fields [59])

$$S^{\text{mic}} = 1 - it\sqrt{\frac{2m_L}{2E_L}}\sqrt{\frac{2m'_L}{2E'_L}}\sqrt{\frac{1}{2\omega_\pi}}\frac{1}{\mathcal{V}^{3/2}}(2\pi)^4\delta(P_{\text{in}} - P_{\text{out}}),$$

$$(14)$$

with m_L, E_L, m'_L, and E'_L the masses (constituent) of the incoming and outgoing light quarks, $\mathcal{V}$ the volume of the box where states are normalized to unity, and ω_π the pion energy. At the macroscopic level we have for the K^{*+} and B^{*+}

$$S^{\text{mac}}_{K^*} = 1 - it_{K^*}\frac{1}{\sqrt{2\omega_{K^*}}}\frac{1}{\sqrt{2\omega_K}}\frac{1}{\sqrt{2\omega_\pi}}\frac{1}{\mathcal{V}^{3/2}}(2\pi)^4\delta(P_{\text{in}} - P_{\text{out}}),$$

$$(15)$$

$$S^{\text{mac}}_{B^*} = 1 - it_{B^*}\frac{1}{\sqrt{2\omega_{B^*}}}\frac{1}{\sqrt{2\omega_B}}\frac{1}{\sqrt{2\omega_\pi}}\frac{1}{\mathcal{V}^{3/2}}(2\pi)^4\delta(P_{\text{in}} - P_{\text{out}}).$$

$$(16)$$
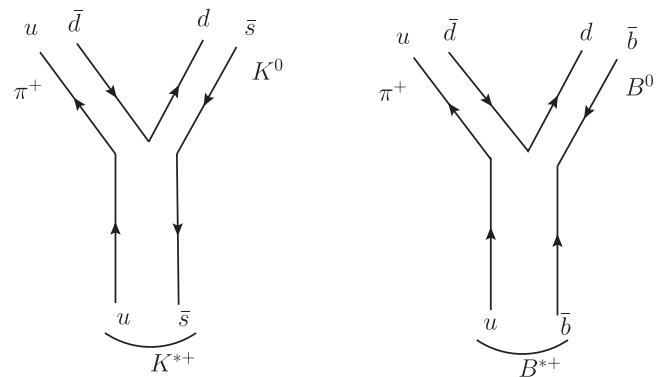
FIG. 5.   Diagram of the transition $K^{*+} \to K^0\pi^+$ (left) and $B^{*+} \to B^0\pi^+$ (right).

These considerations are commonplace in the study of three-body systems in the fixed center approximation [60,61]. Equations (14–16) allow one to relate t_{B^*} and t_{K^*} with the macroscopic t amplitude, but, since we have t_{K^*} given by the effective Lagrangian of Eq. (11), we can obtain t_{B^*} in terms of t_{K^*} by means of

$$\frac{t_{B^*}}{t_{K^*}} \equiv \frac{\sqrt{m_{B^*} m_B}}{\sqrt{m_{K^*} m_K}} \simeq \frac{m_{B^*}}{m_{K^*}}. \tag{17}$$

For a B^* at rest, as we shall assume in our evaluations, t is proportional to $\vec{\epsilon} \cdot \vec{q}$, with $\vec{q}$ the pion momentum and $\vec{\epsilon}$ the polarization vector of the vector meson (corrections of the order of $|\vec{p}_{B^*}|/m_{B^*}$ coming next can be safety neglected). It is interesting to compare what we get in our approach to the results of Ref. [58]. In Ref. [58], the width for $B^{*+} \to B^0 \pi^+$ (or $D^{*+} \to D^0 \pi^+$) is given by

$$\Gamma = \frac{g_H^2}{6\pi \tilde{f}_\pi^2} |\vec{p}_\pi|^3, \tag{18}$$

with g_H the coupling appearing in the heavy hadron Lagrangian and $\tilde{f}_\pi = \sqrt{2} f_\pi$. For the same amplitude, our approach, considering Eq. (17), is given by

$$\Gamma = \frac{1}{6\pi} \frac{1}{m_{B^*}^2} g^2 \left(\frac{m_{B^*}}{m_{K^*}}\right)^2 |\vec{p}_\pi|^3. \tag{19}$$

By taking $g^2/m_{K^*}^2 = (m_V/2f_\pi m_{K^*})^2 \equiv \frac{1}{4f_\pi^2}$, we have the relationship

$$\frac{g_H^2}{2} \equiv \frac{1}{4}; \qquad g_H = \frac{1}{\sqrt{2}}. \tag{20}$$

The same result would appear if we use another heavy vector decay like D^*. Our approach, with the consideration of the field normalizations, leads to a g_H independent of flavor and furthermore provides a value for it of $(\sqrt{2})^{-1}$. This value is in good agreement with the latest lattice QCD result [62] for the $B^* \to B\pi$ decay

$$g_H = 0.57 \pm 0.1. \tag{21}$$

After this reformulation of the essence of the heavy quark symmetry, let us take a step forward and see what happens for the exchange of light vector mesons in the local hidden gauge approach. In Fig. 1, the PPV (or VVV) upper vertex gives rise to $\omega_p + \omega'_p$ [the factor $2\sqrt{s} - M_{B1} - M_{B2}$ of Eq. (1) is the relativistic version of this magnitude]. If we compare now $\bar{K}N \to \bar{K}N$ with $\bar{B}N \to \bar{B}N$, the ratio of amplitudes is given again by Eq. (17), substituting the energies by those involved here:

$$\frac{t'_B}{t'_K} = \frac{\omega_B}{\omega_K}, \tag{22}$$

but now t'_K is proportional to $\omega_K + \omega'_K$ in the local hidden gauge approach, and thus

$$t'_B \propto \frac{\omega_B}{\omega_K} \cdot 2\omega_K \equiv 2\omega_B. \tag{23}$$

Hence, the t'_B amplitude in this case is the same one as t'_K but substituting ω_K by ω_B. This is exactly what the extension of the local hidden gauge approach to the B sector gives if one simply substitutes the s quark by the b quark in the SU(3) Lagrangian [40], and it avoids having to invoke SU(4) arguments as often is done to justify this result.

Now we come back to the evaluation of the box diagrams of Fig. 3. The vertex for the $I = 0$ transition $\bar{B}N \to \bar{B}^*N$ of Fig. 4, considering the Yukawa coupling for the πNN vertex, is given by

$$-it = -\frac{3}{\sqrt{2}} g \frac{m_{B^*}}{m_{K^*}} (q + P_{\text{in}})_\mu \epsilon^\mu \frac{1}{q^2 - m_\pi^2} \frac{D+F}{2f_\pi} \vec{\sigma} \cdot \vec{q}, \tag{24}$$

with $D = 0.75$ and $F = 0.51$ [63], and, since $P_{\text{in}} = q + P_{\text{out}}$ and $P_{\text{out}} \cdot \epsilon = 0$ plus $\epsilon^0 \approx 0$, we get effectively

$$-it = \frac{6}{\sqrt{2}} g \frac{m_{B^*}}{m_{K^*}} \vec{q} \cdot \vec{\epsilon} \frac{1}{q^2 - m_\pi^2} \frac{D+F}{2f_\pi} \vec{\sigma} \cdot \vec{q}. \tag{25}$$

In addition to the pion exchange of Fig. 4, we have the Kroll-Ruderman contact term, depicted in Fig. 6. Following Refs. [54,64], in order to get the Kroll-Ruderman term, we must substitute in Eq. (24) $\epsilon_\mu (q + P_{\text{in}})^\mu \frac{1}{q^2 - m_\pi^2} \vec{\sigma} \cdot \vec{q}$ by $-\vec{\sigma} \cdot \vec{q}$. Then, we must evaluate the diagrams of Fig. 7, and we obtain

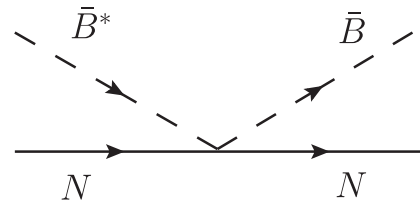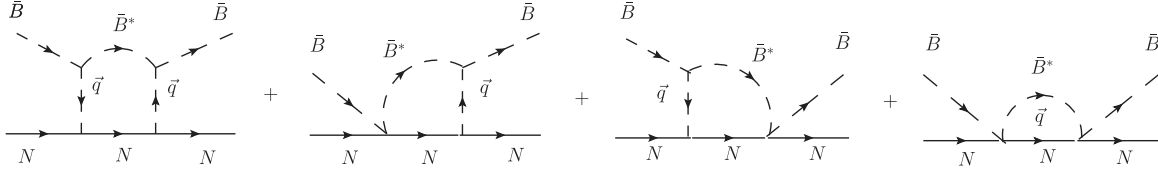$$\delta V = \delta V^{PP} + 2\delta V^{PC} + \delta V^{CC}, \tag{26}$$

where

FIG. 6. Diagram of the Kroll-Ruderman term.

FIG. 7.   All of the diagrams for the $\bar{B}^*N$ in the intermediate state.

$$-i\delta V^{PP} = \int \frac{d^4q}{(2\pi)^4} \left(\frac{m_{B^*}}{m_{K^*}}\right)^2$$

$$\times g \left(\frac{6}{\sqrt{2}}\vec{\epsilon}\cdot\vec{q}\,\frac{1}{q^{02}-\vec{q}^2-m_\pi^2}\frac{D+F}{2f_\pi}\vec{\sigma}\cdot\vec{q}\right)$$

$$\times (-g)\left(\frac{6}{\sqrt{2}}\vec{\epsilon}\cdot\vec{q}\,\frac{1}{q^{02}-\vec{q}^2-m_\pi^2}\frac{D+F}{2f_\pi}\vec{\sigma}\cdot\vec{q}\right)$$

$$\times i\,\frac{1}{2\omega_{B^*}(\vec{q})}\frac{1}{P_{\text{in}}^0-q^0-\omega_{B^*}(\vec{q})+i\epsilon}$$

$$\times i\,\frac{M_N}{E_N(\vec{q})}\frac{1}{K_{\text{in}}^0+q^0-E_N(\vec{q})+i\epsilon}, \tag{27}$$

$$-i\delta V^{PC} = \int \frac{d^4q}{(2\pi)^4} \left(\frac{m_{B^*}}{m_{K^*}}\right)^2 g\left(\frac{3}{\sqrt{2}}\frac{D+F}{2f_\pi}\vec{\sigma}\cdot\vec{\epsilon}\right)$$

$$\times (-g)\left(\frac{6}{\sqrt{2}}\vec{\epsilon}\cdot\vec{q}\,\frac{1}{q^{02}-\vec{q}^2-m_\pi^2}\frac{D+F}{2f_\pi}\vec{\sigma}\cdot\vec{q}\right)$$

$$\times i\,\frac{1}{2\omega_{B^*}(\vec{q})}\frac{1}{P_{\text{in}}^0-q^0-\omega_{B^*}(\vec{q})+i\epsilon}$$

$$\times i\,\frac{M_N}{E_N(\vec{q})}\frac{1}{K_{\text{in}}^0+q^0-E_N(\vec{q})+i\epsilon}, \tag{28}$$

$$-i\delta V^{CC} = \int \frac{d^4q}{(2\pi)^4} \left(\frac{m_{B^*}}{m_{K^*}}\right)^2 g\left(\frac{3}{\sqrt{2}}\frac{D+F}{2f_\pi}\vec{\sigma}\cdot\vec{\epsilon}\right)$$

$$\times (-g)\left(\frac{3}{\sqrt{2}}\frac{D+F}{2f_\pi}\vec{\sigma}\cdot\vec{\epsilon}\right)$$

$$\times i\,\frac{1}{2\omega_{B^*}(\vec{q})}\frac{1}{P_{\text{in}}^0-q^0-\omega_{B^*}(\vec{q})+i\epsilon}$$

$$\times i\,\frac{M_N}{E_N(\vec{q})}\frac{1}{K_{\text{in}}^0+q^0-E_N(\vec{q})+i\epsilon}. \tag{29}$$

Equations (26–29) can be further simplified by considering that $(\vec{\sigma}\cdot\vec{q})(\vec{\sigma}\cdot\vec{q}) = \vec{q}^2$, resorting to symmetry properties

$$q_i q_j \to \frac{1}{3}\vec{q}^2\delta_{ij}, \tag{30}$$

and further considering that, as shown in Ref. [54],

$$\langle PN|\vec{\sigma}\cdot\vec{\epsilon}|VN\rangle \equiv \sqrt{3}\delta_{J,1/2}. \tag{31}$$

Thus in the $\bar{B}N \to \bar{B}^*N \to \bar{B}N$ transition, in $L=0$, we have $J=1/2$, and the Kroll-Ruderman term contributes together with the pion in flight term (pion exchange).

In the $\bar{B}^*N \to \bar{B}N \to \bar{B}^*N$, we can have $L=0, 2$ in the intermediate $\bar{B}N$ states. Now in $\bar{B}^*N$ we can have $J=1/2$, $3/2$. If $J=1/2$, then $L=0$ for the $\bar{B}N$ intermediate states, and both the pion in flight and Kroll-Ruderman terms contribute. The formulas are then formally the same as for the $\bar{B}N \to \bar{B}^*N \to \bar{B}N$ box diagram, changing appropriately the masses. However, if we have $J=3/2$, then the Kroll-Ruderman term does not contribute, and the pion in flight δV^{PP} with $L=2$ contributes the same as for $L=0$. Furthermore, before we had the vertices $(\vec{\epsilon}\cdot\vec{q})(\vec{\epsilon}\cdot\vec{q})$ and we must sum over polarizations of the $\vec{\epsilon}$, so one gets the factor $\vec{q}^2$, but in the $\bar{B}^*N \to \bar{B}N \to \bar{B}^*N$ transition we have $(\vec{\epsilon}\cdot\vec{q})(\vec{\epsilon}'\cdot\vec{q}')$ and $\vec{\epsilon}, \vec{\epsilon}'$ are the external polarization vectors. The symmetry of the integral allows us to use Eq. (30), and then we get $\frac{1}{3}\vec{q}^2\vec{\epsilon}\cdot\vec{\epsilon}'$, so we get a factor of $\frac{1}{3}$ in the PP term of Eq. (27). The scalar $\vec{\epsilon}\cdot\vec{\epsilon}'$ factor tells us that this term is the same for $J=1/2, 3/2$.

One further step to simplify the equations comes from performing the q^0 integration analytically. After all this is done, we obtain the following results for the $\bar{B}^*N \to \bar{B}N \to \bar{B}^*N$ box diagram:

$$J=1/2: \ \delta V = FAC\left(\frac{\partial}{\partial m_\pi^2}I_1' + 2I_2' + I_3'\right), \tag{32}$$

$$J=3/2: \ \delta V = FAC\left(\frac{\partial}{\partial m_\pi^2}I_1'\right), \tag{33}$$

where

$$I_1' = \int \frac{d^3q}{(2\pi)^3}\frac{4}{3}\vec{q}^4\frac{1}{2\omega_B(\vec{q})}\frac{M_N}{E_N(\vec{q})}\frac{Num}{Den}, \tag{34}$$

$$I_2' = \int \frac{d^3q}{(2\pi)^3}2\vec{q}^2\frac{1}{2\omega_B(\vec{q})}\frac{M_N}{E_N(\vec{q})}\frac{Num}{Den}, \tag{35}$$

$$I_3' = \int \frac{d^3q}{(2\pi)^3}\frac{3}{2\omega_B(\vec{q})}\frac{M_N}{E_N(\vec{q})}$$

$$\times \frac{1}{P_{\text{in}}^0+K_{\text{in}}^0-E_N(\vec{q})-\omega_B(\vec{q})+i\epsilon}, \tag{36}$$

with

TABLE XVI. Poles with a box diagram in coupled channels $\bar{B}^*N$, $\rho\Sigma_b$, $\omega\Lambda_b$, and $\phi\Lambda_b$ in $I = 0$ as a function of V and $q_{\max}$ (unit, MeV).

$q_{\max}$	700	750	776	800	850
$J = 1/2$	$5991.9 + i0$	$5939.2 + i0$	$5910.7 + i0$	$5884.0 + i0$	$5827.4 + i0$
	$6364.2 + i1.4$	$6332.6 + i1.4$	$6316.6 + i1.4$	$6301.1 + i1.4$	$6273.0 + i1.2$
$J = 3/2$	$5998.8 + i0$	$5948.0 + i0$	$5920.7 + i0$	$5895.1 + i0$	$5840.9 + i0$
	$6363.5 + i2.1$	$6331.7 + i2.0$	$6315.7 + i1.9$	$6301.2 + i1.7$	$6272.1 + i1.2$

TABLE XVII. Poles with a box diagram in coupled channels $\bar{B}N$, $\pi\Sigma_b$, and $\eta\Lambda_b$ in $I = 0$ as a function of V and $q_{\max}$ (unit, MeV).

$q_{\max}$	700	750	776	800	850
$J = 1/2$	$5902.6 + i0$	$5850.1 + i0$	$5820.9 + i0$	$5793.3 + i0$	$5734.4 + i0$
	$5985.6 + i29.1$	$5974.1 + i26.8$	$5969.5 + i24.6$	$5965.8 + i22.3$	$5959.5 + i17.3$

$$FAC = \frac{9}{2} g^2 \left(\frac{m_{B^*}}{m_{K^*}}\right)^2 \left(\frac{F+D}{2f_\pi}\right)^2, \qquad (37)$$

$$Num = K^0_{\text{in}} - E_N(\vec{q}) - 2\omega_\pi(\vec{q}) - \omega_B(\vec{q}) + P^0_{\text{in}}, \quad (38)$$

$$Den = 2\omega_\pi(\vec{q})[P^0_{\text{in}} - \omega_\pi(\vec{q}) - \omega_B(\vec{q}) + i\epsilon]$$
$$\times [K^0_{\text{in}} - E_N(\vec{q}) - \omega_\pi(\vec{q}) + i\epsilon]$$
$$\times [P^0_{\text{in}} + K^0_{\text{in}} - E_N(\vec{q}) - \omega_B(\vec{q}) + i\epsilon], \quad (39)$$

with P^0_{in}, K^0_{in} the incoming $\bar{B}^*$, N energies.

For the case of the $\bar{B}N \to \bar{B}^*N \to \bar{B}N$ box diagram, we have only the $J = 1/2$ case, and the formula is like the former one for $J = 1/2$ exchanging accordingly the masses of $B^* \leftrightarrow B$ and considering the factor of 3 extra in V^{PP}. Thus, we have

$$J = 1/2: \delta V = FAC\left(\frac{\partial}{\partial m_\pi^2} I_1 + 2I_2 + I_3\right), \quad (40)$$

where

$$I_1 = \int \frac{d^3q}{(2\pi)^3} 4\vec{q}^4 \frac{1}{2\omega_{B^*}(\vec{q})} \frac{M_N}{E_N(\vec{q})} \frac{Num}{Den}, \quad (41)$$

$$I_2 = \int \frac{d^3q}{(2\pi)^3} 2\vec{q}^2 \frac{1}{2\omega_{B^*}(\vec{q})} \frac{M_N}{E_N(\vec{q})} \frac{Num}{Den}, \quad (42)$$

$$I_3 = \int \frac{d^3q}{(2\pi)^3} \frac{3}{2\omega_{B^*}(\vec{q})} \frac{M_N}{E_N(\vec{q})}$$
$$\times \frac{1}{P^0_{\text{in}} + K^0_{\text{in}} - E_N(\vec{q}) - \omega_{B^*}(\vec{q}) + i\epsilon}, \quad (43)$$

with Num and Den having the same expressions but in terms of the proper energies and masses. In the Yukawa vertex, it is customary to include a monopole form factor to agree with the NN peripheral partial waves [65], and thus we introduce a factor of

$$FF(\vec{q}) = \left(\frac{\Lambda^2}{\Lambda^2 + \vec{q}^2}\right)^2, \qquad (44)$$

with $\Lambda \simeq 1$ GeV, which we include in the integrands of Eqs. (34–36), (41–43).

To go to the second Riemann sheet with the box contribution δV, we can do a similar thing as in Eq. (9). Yet, when $\sqrt{s}$ is real, $G_l^{II} \equiv (G_l^I)^*$, and this is also the case, quite accurately, when we are close to the real axis. In view of this, and the small contribution of the intermediate $\bar{B}N$ states to the width, we use the prescription $\delta V \to (\delta V)^*$ to go to the second Riemann sheet. In practice, this is equivalent to changing $+i\epsilon \to -i\epsilon$ in the factors of Den of Eq. (39).[1]

Once the formalism has been described, we show the results of including δV in the approach in Tables XVI and XVII.

It is interesting to compare the results of Table XVI with those of Table XIV. At 750 MeV the box diagram reduces the mass of the state by about 30 MeV for $J = 1/2$ and 20 MeV for $J = 3/2$. We can see that the value of the masses is rather sensitive to the value $q_{\max}$ used. However, it is interesting to remark that the splitting of energies between the $J = 1/2$ and $J = 3/2$ levels is about 10 MeV, rather independent of the cutoff used. We can thus see that the mixing of $\bar{B}^*N$ and $\bar{B}N$ states leads naturally to two states, nearly degenerate in spin, only separated by about 10 MeV, like the $\Lambda_b(5912)$ and $\Lambda_b(5920)$. If we fine-tune $q_{\max}$ to get the right binding, we find $q_{\max} = 776$ MeV, where the energy of the $J = 1/2$ state is 5910 MeV, and the

---

[1]In this case, only the last factor of Eq. (39) can produce a singularity, and the analytical structure is like the one G. For the $\bar{B}^*\Delta \to \bar{B}N \to \bar{B}^*\Delta$ case, that we shall study later, also the second-to-last factor can lead to a singularity from $\Delta \to \pi N$, but the binding of the $\bar{B}^*\Delta$ state does not give much phase space for it. Hence, we apply the same rule. At the end, we check that the width that comes out from the complex pole coincides with that of $|T|^2$ in the real axis.

TABLE XVIII. The coupling constants to various channels for certain poles in the $I = 1$ sector of $\bar{B}N$ and coupled channels.

$6002.8 + i66.2$	$\bar{B}N$	$\pi\Sigma_b$	$\pi\Lambda_b$	$\eta\Sigma_b$
g_i	$5.69 + i1.62$	$1.80 + i1.00$	$0.39 + i0.21$	$0.37 + i0.20$
$g_i G_i^{II}$	$-8.60 - i4.12$	$-72.70 - i12.65$	$-16.12 + i5.73$	$-2.95 - i2.01$

$6179.4 + i61.4$	$\bar{B}N$	$\pi\Sigma_b$	$\pi\Lambda_b$	$\eta\Sigma_b$
g_i	$6.76 - i3.03$	$0.30 + i0.80$	$1.11 - i0.03$	$1.07 - i0.03$
$g_i G_i^{II}$	$-21.71 + i1.38$	$-30.00 - i13.31$	$-14.96 + i47.71$	$-12.74 - i1.63$

one of the $J = 3/2$ state 5920 MeV. We also observe that the higher-energy state, around 6300 MeV, has been practically not affected by the box diagram, which is most logical since this state couples weakly to $\bar{B}^*N$.

For the $\bar{B}N$ state of Table XVII, comparing it with the results of Table VIII, the box diagram has reduced the energy by about 50 MeV at $q_{max} = 750$ MeV. The upper level energy is increased by about 15 MeV for this value of q_{max}.

VI. $I = 1$ STATES

With the cutoff obtained to reproduce the mass of the $\Lambda_b(5912)$ state, we proceed now to evaluate the states corresponding to Tables II, IV, XI, and XII, which are mostly bound states of $\bar{B}N(I = 1, J^P = 1/2^-)$, $\bar{B}\Delta(I = 1, J^P = 3/2^-)$, $\bar{B}^*N(I = 1, J^P = 1/2^-, 3/2^-)$, and $\bar{B}^*\Delta(I = 1, J^P = 1/2^-, 3/2^-, 5/2^-)$. The results can be seen in Tables XVIII–XXI with $q_{max} = 776$ MeV, together with the couplings to the different coupled channels.

With respect to their thresholds, the binding energies for the $\bar{B}N$ channel are now smaller than for $I = 0$, as we anticipated in view of the smaller C_{ij} coefficients, but for $\bar{B}\Delta$ the binding is bigger than for the $\bar{B}N$ state, as discussed earlier. We again see that we get two states in each one of the cases but also notice that there is more mixture of the states than for $I = 0$. In the case of the $\bar{B}N$ channels, the lower state is clearly dominated by $\pi\Sigma_b$. For the $\bar{B}\Delta$ channels, the upper state is dominated by $\pi\Sigma_b^*$. For the $\bar{B}^*N$ channels, the lower state is dominated by $\bar{B}^*N$ and the higher one by $\rho\Sigma_b$. For the $\bar{B}^*\Delta$ channels, the lower state is dominated by $\bar{B}^*\Delta$ and the upper one by $\rho\Sigma_b^*$.
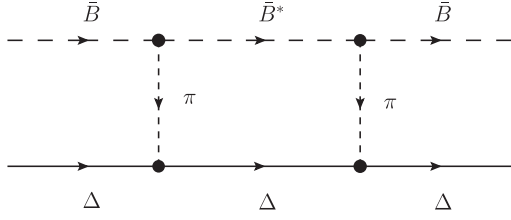
VII. BOX DIAGRAM FOR $I = 1$ STATES

We now evaluate the contribution of the box diagram to the $I = 1$ states made from $\bar{B}N$, $\bar{B}^*N$, $\bar{B}\Delta$, and $\bar{B}^*\Delta$.
(a) $\bar{B}N$, $I = 1$.—The isospin $I = 1$ state is now

$$|\bar{B}N; I = 1, I_3 = 0\rangle = \frac{1}{\sqrt{2}}(|\bar{B}^0 n\rangle - |\bar{B}^- p\rangle). \quad (45)$$

TABLE XIX. The coupling constants to various channels for certain poles in the $I = 1$ sector of $\bar{B}\Delta$ and coupled channels.

$5971.9 + i0$	$\bar{B}\Delta$	$\pi\Sigma_b^*$	$\eta\Sigma_b^*$
g_i	10.79	0.61	0.85
$g_i G_i^{II}$	-10.89	-16.51	-6.69

$6073.0 + i77.2$	$\bar{B}\Delta$	$\pi\Sigma_b^*$	$\eta\Sigma_b^*$
g_i	$7.67 - i5.14$	$1.43 + i1.36$	$0.81 - i0.36$
$g_i G_i^{II}$	$-9.59 + i4.83$	$-70.37 - i20.89$	$-7.87 + i2.27$

TABLE XXI. The coupling constants to various channels for certain poles in the $I = 1$ sector of $\bar{B}^*\Delta$ and coupled channels.

$6049.2 + i0$	$\bar{B}^*\Delta$	$\rho\Sigma_b^*$	$\omega\Sigma_b^*$	$\phi\Sigma_b^*$
g_i	21.14	0.85	1.03	1.46
$g_i G_i^{II}$	-22.11	-4.70	-5.66	-5.30

$6491.9 + i0$	$\bar{B}^*\Delta$	$\rho\Sigma_b^*$	$\omega\Sigma_b^*$	$\phi\Sigma_b^*$
g_i	0.66	3.76	0.13	0.18
$g_i G_i^{II}$	-2.19	-50.69	-1.71	-1.20

TABLE XX. The coupling constants to various channels for certain poles in the $I = 1$ sector of $\bar{B}^*N$ and coupled channels.

$6202.1 + i0$	$\bar{B}^*N$	$\rho\Sigma_b$	$\rho\Lambda_b$	$\omega\Sigma_b$	$\phi\Sigma_b$
g_i	7.29	1.22	1.05	0.59	0.83
$g_i G_i^{II}$	-20.66	-8.67	-11.20	-4.11	-3.62

$6477.2 + i5.0$	$\bar{B}^*N$	$\rho\Sigma_b$	$\rho\Lambda_b$	$\omega\Sigma_b$	$\phi\Sigma_b$
g_i	$0.21 - i0.62$	$3.68 - i0.08$	$0.25 + i0.12$	$0.14 + i0.07$	$0.20 + i0.10$
$g_i G_i^{II}$	$4.23 + i2.05$	$-50.58 + i0.19$	$-9.39 + i2.89$	$-1.85 - i0.94$	$-1.29 - i0.64$

FIG. 8. Diagrammatic representation of the transition of $\bar{B}\Delta \to \bar{B}^*\Delta \to \bar{B}\Delta$.

The counting of isospin done before can be repeated, and we simply find that a factor of $\frac{3}{\sqrt{2}}$ gets converted in $\frac{1}{\sqrt{2}}$ in the $\bar{B}N \to \bar{B}^*N$ transition. We thus get a factor of 9 smaller contribution than for $I = 0$ from the box, and we neglect it.

(b) $\bar{B}^*N$, $I = 1$.—We have the same suppression factor as before, and we also neglect it.

(c) $\bar{B}\Delta$, $I = 1$.—The state of $\bar{B}\Delta$ with $I = 1$ is given by

$$|\bar{B}\Delta; I = 1, I_3 = 1\rangle = \sqrt{\frac{3}{4}}|\bar{B}^-\Delta^{++}\rangle + \sqrt{\frac{1}{4}}|\bar{B}^0\Delta^+\rangle. \quad (46)$$

The diagram under contribution is now in Fig. 8. We must also substitute $\frac{f}{m_\pi}\vec{\sigma}\cdot\vec{q}\tau^\lambda$ in the case of nucleons by $\frac{f_\Delta}{m_\pi}\vec{S}_\Delta\cdot\vec{q}T_\Delta^\lambda$, where $\vec{S}_\Delta$ and $\vec{T}_\Delta$ are the ordinary spin and isospin matrices, respectively, of the Δ.
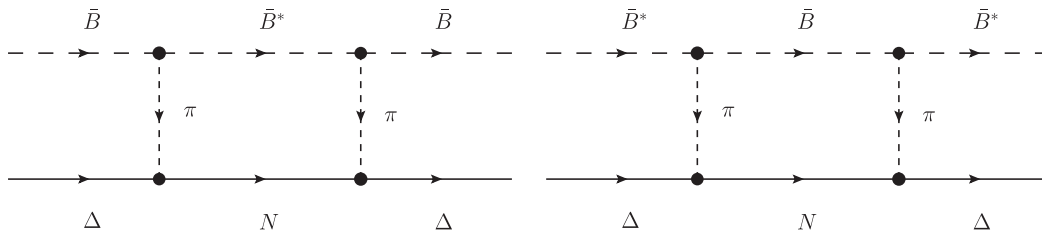
We have [66]

$$\frac{f_\Delta}{f} = \frac{4}{5} \quad \left(\text{where } \frac{f}{m_\pi} = \frac{F+D}{2f}\right). \quad (47)$$

Using the appropriate Clebsch-Gordan coefficient for $\vec{T}_\Delta$, we find that the term corresponding to the box in Fig. 8 is now given by

$$\delta V = FAC\frac{\partial \tilde{I}_1}{\partial m_\pi^2}, \quad (48)$$

where

$$\tilde{I}_1 = \frac{5}{9}\int\frac{d^3q}{(2\pi)^3}4\vec{q}^4\frac{1}{2\omega_{B^*}(\vec{q})}\frac{M_\Delta}{E_\Delta(\vec{q})}\frac{Num}{Den}, \quad (49)$$

with Num and Den the expressions of Eqs. (38) and (39), respectively, but putting the appropriate masses.

(d) $\bar{B}^*\Delta$, $I = 1$.—In this case, we proceed as before, and everything is formulated in the same way but now $I'_1 \to \tilde{I}'_1$, with

$$\tilde{I}'_1 = \frac{5}{9}\int\frac{d^3q}{(2\pi)^3}\frac{4}{3}\vec{q}^4\frac{1}{2\omega_B(\vec{q})}\frac{M_\Delta}{E_\Delta(\vec{q})}\frac{Num}{Den}. \quad (50)$$

To reach this formula, we have made an average over the spins of the initial Δ, taking the same initial and final third spin component of the Δ. This is in consonance with the fact that, since we have a reduction factor of about $1/2$, the splitting of spin levels is now smaller than for $\bar{B}^*N$, and accepting uncertainties larger than 5 MeV we do not worry about it. Consequently, we do not evaluate the I_2, I_3, I'_2, and I'_3 terms that produced the spin splitting.

VIII. FURTHER DECAY CHANNELS OF $\bar{B}\Delta$ AND $\bar{B}^*\Delta$

In this section, we evaluate the box diagram corresponding to Fig. 9. We thus consider the intermediate $\bar{B}N$ or $\bar{B}^*N$ channels. Should the binding $\bar{B}\Delta$ and $\bar{B}^*\Delta$ states be not bigger than the Δ and N mass differences, $\bar{B}N$ and $\bar{B}^*N$ would provide decay channels of the states. In principle, we should also consider the $\bar{B}\Delta$ and $\bar{B}^*\Delta$ intermediate states for the $\bar{B}N$ and $\bar{B}^*N$ states, but, considering the binding, these intermediate states are about 600 MeV away in energy, and we do not consider them. The changes are also simple: We must substitute

$$\frac{f}{m_\pi}\vec{\sigma}\cdot\vec{q}\tau^\lambda \to \frac{f_{\pi N\Delta}}{m_\pi}\vec{S}\cdot\vec{q}T^\lambda, \quad (51)$$

where now $\vec{S}(\vec{T})$ is the transition spin (isospin) operator from spin (isospin) $3/2$ to $1/2$, with the normalization for S_μ^+ in the spherical basis

$$\langle 3/2M|S_\mu^+|1/2m\rangle = \mathcal{C}(1/2\,1\,3/2; m_\mu M), \quad (52)$$

FIG. 9. Diagrammatic representation of the $\bar{B}^*N$ in the intermediate state (left) and the $\bar{B}N$ in the intermediate state (right).

with $C(\cdot)$ a Clebsch-Gordan coefficient, and we have the property [67]

$$\sum_M S_i |M\rangle\langle M|S_j = \frac{2}{3}\delta_{ij} - i\frac{1}{3}\epsilon_{ijk}\sigma_k, \qquad (53)$$

for S_i, S_j in the Cartesian basis. Also from Ref. [67], we take $f_{\pi N\Delta}/f = 2.25$. For the isospin transition, in addition to the $I = 1$ $\bar{B}\Delta$ state of Eq. (46), we need

$$|\bar{B}N; I = 1, I_3 = 1\rangle = |\bar{B}^0 p\rangle. \qquad (54)$$

The $\pi^0 p\Delta^+$ vertex for T_Δ^λ gives us $\sqrt{2/3}$, and the $\pi^+ p\Delta^{++}$ gives us (-1) (recall phase used $|\pi^+\rangle = -|1,1\rangle$).

Once again, making the average over Δ spins as before, we obtain the results for δV_2 given by the same formalism as before, substituting

$$I_1 \to \tilde{I}_1 = \frac{8}{81}\left(\frac{f_{\pi N\Delta}}{f}\right)^2 \int \frac{d^3q}{(2\pi)^3} 4\vec{q}^{\,4} \frac{1}{2\omega_{B^*}(\vec{q})E_N(\vec{q})} \frac{M_N}{Den} \frac{Num}{}, \qquad (55)$$

for the $\bar{B}\Delta \to \bar{B}^*N \to \bar{B}\Delta$ process, and

$$I_1' \to \tilde{I}_1' = \frac{8}{81}\left(\frac{f_{\pi N\Delta}}{f}\right)^2 \int \frac{d^3q}{(2\pi)^3} \frac{4}{3}\vec{q}^{\,4} \frac{1}{2\omega_B(\vec{q})E_N(\vec{q})} \frac{M_N}{Den} \frac{Num}{}, \qquad (56)$$

for the $\bar{B}^*\Delta \to \bar{B}N \to \bar{B}^*\Delta$ process, with Num and Den given by Eqs. (38) and (39), respectively, but substituting the masses by the appropriate ones.

We show our results with the contribution of box diagrams, seen in Figs. 8 and 9, in Tables XXII and XXIII for the $\bar{B}\Delta$ and $\bar{B}^*\Delta$ and their coupled channels.

We can see that the effect of the box with $\bar{B}\Delta$ or $\bar{B}^*\Delta$ intermediate states is a reduction of the mass of the lower

state by about 10–15 MeV, with an extra reduction of about 15–25 MeV from the box with intermediate $\bar{B}N$ and $\bar{B}^*N$ states. The upper state is not much modified by the box diagrams.

IX. SUMMARY OF THE RESULTS

Finally, since we have many intermediate results, we summarize here the final results that we get for the states, with $q_{max} = 776$ MeV, which we used to fix one of the Λ_b energies. The results are shown in Table XXIV, where we also write for a quick intuition the main channel of the state.

In summary, we predict six states with $I = 0$, two of them corresponding to the $\Lambda_b(5912)$ and $\Lambda_b(5920)$, and eight states with $I = 1$. The energies of the states range from about 5800 to 6500 MeV.

It is interesting to compare the results obtained here with those of Ref. [31]. In this later work, the same interaction as here is used for the main diagonal channels, but the transition between different coupled channels is not obtained through vector or pion exchange as done here, but by invoking a combined SU(6) and heavy quark spin symmetry. In Ref. [31], the states of $I = 1$ are not investigated, but for $I = 0$ four states are obtained; two of them, with $J = 1/2$, $3/2$, are also associated to the $\Lambda_b(5912)$ and $\Lambda_b(5920)$. In spite of the differences in the input, there are common features in the results. The two states associated to the $\Lambda_b(5912)$ and $\Lambda_b(5920)$ exhibit, as here, a substantial coupling to $\bar{B}^*N$. There is also a $1/2^-$ state in Ref. [31] at 5797 MeV which we find at 5820 MeV, only 33 MeV higher, and another state at 6009 MeV that we find at 5969 MeV, 40 MeV below. The mostly $\rho\Sigma_b$ state found here at 6316 MeV, basically degenerate in $J = 1/2, 3/2$, was either not found or not searched for in Ref. [31] because of its higher mass. The qualitative agreement between the results of the two approaches is remarkable and gives further support to the common predictions. In addition, we have investigated states of $I = 1$, and

TABLE XXII. Poles with a box diagram in the $I = 1$ sector of $\bar{B}\Delta$ and its coupled channels with $q_{max} = 776$ MeV: δV_1 is the $\bar{B}^*\Delta$ box, and δV_2 is the $\bar{B}^*N$ box (unit, MeV).

No box	$V + \delta V_1$	$V + \delta V_2$	$V + \delta V_1 + \delta V_2$
$5971.9 + i0$	$5957.8 + i0$	$5949.4 + i0$	$5932.9 + i0$
$6073.0 + i77.2$	$6069.1 + i80.7$	$6066.3 + i81.7$	$6063.8 + i83.5$

TABLE XXIII. Poles with a box diagram in the $I = 1$ sector of $\bar{B}^*\Delta$ and its coupled channels with $q_{max} = 776$ MeV: δV_1 is the $\bar{B}\Delta$ box, and δV_2 is the $\bar{B}N$ box (unit, MeV).

No box	$V + \delta V_1$	$V + \delta V_2$	$V + \delta V_1 + \delta V_2$
$6049.2 + i0$	$6039.1 + i0$	$6032.2 + i0$	$6022.9 + i0$
$6491.9 + i0$	$6491.4 + i0$	$6493.0 + i1.0$	$6491.7 + i0.8$

TABLE XXIV. Energies and widths of the states obtained and the channels to which the states couple most strongly.

Main channel	J	I	(E,Γ) [MeV]	Exp.
$\bar{B}N$	1/2	0	5820.9, 0	
$\pi\Sigma_b$	1/2	0	5969.5, 49.2	
$\bar{B}^*N$	1/2	0	5910.7, 0	$\Lambda_b(5912)$
$\bar{B}^*N$	3/2	0	5920.7, 0	$\Lambda_b(5920)$
$\rho\Sigma_b$	1/2	0	6316.6, 2.8	
$\rho\Sigma_b$	3/2	0	6315.7, 3.8	
$\bar{B}N, \pi\Sigma_b$	1/2	1	6179.4, 122.8	
$\pi\Sigma_b$	1/2	1	6002.8, 132.4	
$\bar{B}\Delta, \pi\Sigma_b^*$	3/2	1	5932.9, 0	
$\pi\Sigma_b^*$	3/2	1	6063.8, 167.0	
$\bar{B}^*N$	1/2, 3/2	1	6202.2, 0	
$\rho\Sigma_b$	1/2, 3/2	1	6477.2, 10.0	
$\bar{B}^*\Delta$	1/2, 3/2, 5/2	1	6022.9, 0	
$\rho\Sigma_b^*$	1/2, 3/2, 5/2	1	6491.7, 1.6	

we find quite a few, some of them narrow enough for a clear experimental observation.

X. CONCLUSIONS

In this work, we studied the interaction of $\bar{B}N$, $\bar{B}\Delta$, $\bar{B}^*N$, and $\bar{B}^*\Delta$ states with its coupled channels by using dynamics mapped from the light quark sector to the heavy one. The starting point was to assume that the heavy quarks act as spectators in the dominant terms of the interaction. Then we studied pion exchange and vector exchange and obtained the results of pion exchange in the heavy quark spin symmetric approach combined with results of lattice QCD. The same procedure led us to the standard interaction of the extended local hidden gauge approach from the exchange of light vector mesons. With these elements of the interaction, supplemented with the subleading terms, in the large heavy quark mass counting, obtained from the exchange of heavy mesons in the local hidden gauge approach, we studied the interaction of the $\bar{B}N$, $\bar{B}\Delta$, $\bar{B}^*N$, and $\bar{B}^*\Delta$ with their coupled channels $\pi\Sigma_b$, $\pi\Lambda_b$, and $\eta\Sigma_b$ (for the $\bar{B}N$); $\pi\Sigma_b^*$ and $\eta\Sigma_b^*$ (for the $\bar{B}\Delta$); $\rho\Sigma_b$, $\omega\Lambda_b$, $\phi\Lambda_b$, $\rho\Sigma_b^*$, $\omega\Sigma_b^*$, and $\phi\Sigma_b^*$ (for the $\bar{B}^*N$); and $\rho\Sigma_b^*$, $\omega\Sigma_b^*$, and $\phi\Sigma_b^*$ (for the $\bar{B}^*\Delta$), and we searched for poles of the scattering matrix in different states of spin and isospin. We found six states in $I = 0$, with one of them degenerate in spin $J = 1/2$, $3/2$, and eight states in $I = 1$, less bound, two of them degenerate in spin $J = 1/2$, $3/2$, and two more degenerate in spin $J = 1/2$, $3/2$, $5/2$. The couplings of the states to the different channels were evaluated, together with their wave function at the origin, in order to get a feeling of which are the largest building blocks in those molecular states. In particular, when studying the inter-action of $\bar{B}^*N$ with its coupled channels, we found two states in $I = 0$, degenerate in spin $J = 1/2$, $3/2$, which couple mostly to $\bar{B}^*N$. The degeneracy is broken when the

pion exchange is considered, allowing a mixture with intermediate $\bar{B}N$ states. Then we find that the mass of the states is close to 5910 MeV for natural values of the regularizing cutoff. More important, the splitting between the two states when the pion exchange is considered is found to be of the order of 10 MeV, rather independent of the cutoff used. This feature was considered relevant in view of the existence of the $\Lambda_b(5912)$ and $\Lambda_b(5920)$ states, which are separated by this amount of energy. A fine-tuning of the cutoff was then done to match the exact energy of one of these states, and then it was used subsequently to make predictions in all the other sectors of spin and isospin, leading to the states reported above. We think that the use of realistic dynamics, with strict fulfilment of heavy quark spin-flavor symmetry, makes the results obtained here rather accurate and should serve as a guideline for future experimental searches of baryon states with open beauty.

ACKNOWLEDGMENTS

[1] A. Ali, *Proc. Sci.*, BEAUTY (**2011**) 002.
[2] M. Gersabeck, Mod. Phys. Lett. A **27**, 1230026 (2012).
[3] S. L. Olsen, Prog. Theor. Phys. Suppl. **193**, 38 (2012).
[4] L. Li (BESIII Collaboration), Nucl. Phys. B, Proc. Suppl. **225–227**, 107 (2012).
[5] P. De Simone (LHCb Collaboration), Nucl. Phys. B, Proc. Suppl. **233**, 18 (2012).
[6] P. Palni (CDF Collaboration), Nucl. Phys. B, Proc. Suppl. **233**, 151 (2012).
[7] N. Brambilla *et al.*, Eur. Phys. J. C **71**, 1534 (2011).
[8] E. E. Kolomeitsev and M. F. M. Lutz, Phys. Lett. B **582**, 39 (2004).
[9] L. Maiani, V. Riquer, F. Piccinini, and A. D. Polosa, Phys. Rev. D **72**, 031502 (2005).
[10] F.-K. Guo, P.-N. Shen, H.-C. Chiang, R.-G. Ping, and B.-S. Zou, Phys. Lett. B **641**, 278 (2006).
[11] E. Swanson, Int. J. Mod. Phys. A **21**, 733 (2006); AIP Conf. Proc. **814**, 203 (2006).
[12] J. L. Rosner, J. Phys. Conf. Ser. **69**, 012002 (2007).
[13] D. Gamermann, E. Oset, D. Strottman, and M. J. Vicente Vacas, Phys. Rev. D **76**, 074016 (2007).
[14] M. Nielsen, F. S. Navarra, and S. H. Lee, Phys. Rep. **497**, 41 (2010).
[15] T. Branz, T. Gutsche, and V. E. Lyubovitskij, Phys. Rev. D **80**, 054019 (2009).
[16] E. Klempt and J.-M. Richard, Rev. Mod. Phys. **82**, 1095 (2010).
[17] P. G. Ortega, D. R. Entem, and F. Fernandez, J. Phys. G **40**, 065107 (2013).

[18] C. Hidalgo-Duque, J. Nieves, and M. P. Valderrama, Phys. Rev. D **87**, 076006 (2013).

[19] J. A. Oller, E. Oset, and A. Ramos, Prog. Part. Nucl. Phys. **45**, 157 (2000).

[20] E. Oset, A. Ramos, E. J. Garzon, R. Molina, L. Tolos, C. W. Xiao, J. J. Wu, and B. S. Zou, Int. J. Mod. Phys. E **21**, 1230011 (2012).

[21] J. Hofmann and M. F. M. Lutz, Nucl. Phys. **A763**, 90 (2005).

[22] T. Mizutani and A. Ramos, Phys. Rev. C **74**, 065201 (2006).

[23] L. Tolos, A. Ramos, and T. Mizutani, Phys. Rev. C **77**, 015207 (2008).

[24] J.-J. Wu, R. Molina, E. Oset, and B. S. Zou, Phys. Rev. Lett. **105**, 232001 (2010).

[25] J.-J. Wu, R. Molina, E. Oset, and B. S. Zou, Phys. Rev. C **84**, 015202 (2011).

[26] O. Romanets, L. Tolos, C. Garca-Recio, J. Nieves, L. L. Salcedo, and R. Timmermans, Nucl. Phys. **A914**, 488 (2013).

[27] C. Garcia-Recio, J. Nieves, O. Romanets, L. L. Salcedo, and L. Tolos, Phys. Rev. D **87**, 074034 (2013).

[28] O. Romanets, L. Tolos, C. Garcia-Recio, J. Nieves, L. L. Salcedo, and R. G. E. Timmermans, Phys. Rev. D **85**, 114032 (2012).

[29] C. W. Xiao, J. Nieves, and E. Oset, Phys. Rev. D **88**, 056012 (2013).

[30] J.-J. Wu, L. Zhao, and B. S. Zou, Phys. Lett. B **709**, 70 (2012).

[31] C. Garcia-Recio, J. Nieves, O. Romanets, L. L. Salcedo, and L. Tolos, Phys. Rev. D **87**, 034032 (2013).

[32] C. W. Xiao and E. Oset, Eur. Phys. J. A **49**, 139 (2013).

[33] P. G. Ortega, D. R. Entem, and F. Fernandez, Phys. Lett. B **718**, 1381 (2013).

[34] R. Aaij et al. (LHCb Collaboration), Phys. Rev. Lett. **109**, 172003 (2012).

[35] T. A. Aaltonen et al. (CDF Collaboration), Phys. Rev. D **88**, 071101 (2013).

[36] P. Palni (CDF Collaboration), arXiv:1309.6269.

[37] S. Capstick and N. Isgur, Phys. Rev. D **34**, 2809 (1986).

[38] H. Garcilazo, J. Vijande, and A. Valcarce, J. Phys. G **34**, 961 (2007).

[39] C. Garcia-Recio, V. K. Magas, T. Mizutani, J. Nieves, A. Ramos, L. L. Salcedo, and L. Tolos, Phys. Rev. D **79**, 054004 (2009).

[40] A. Ozpineci, C. W. Xiao, and E. Oset, Phys. Rev. D **88**, 034018 (2013).

[41] J. Nieves and M. P. Valderrama, Phys. Rev. D **84**, 056015 (2011).

[42] Z.-F. Sun, J. He, X. Liu, Z.-G. Luo, and S.-L. Zhu, Phys. Rev. D **84**, 054002 (2011).

[43] M. Bando, T. Kugo, S. Uehara, K. Yamawaki, and T. Yanagida, Phys. Rev. Lett. **54**, 1215 (1985).

[44] M. Bando, T. Kugo, and K. Yamawaki, Phys. Rep. **164**, 217 (1988).

[45] U. G. Meissner, Phys. Rep. **161**, 213 (1988).

[46] E. Oset and A. Ramos, Nucl. Phys. **A635**, 99 (1998).

[47] S. Sarkar, E. Oset, and M. J. Vicente Vacas, Nucl. Phys. **A750**, 294 (2005); **A780**, 90(E) (2006).

[48] E. Oset, A. Ramos, and C. Bennhold, Phys. Lett. B **527**, 99 (2002); **530**, 260(E) (2002).

[49] B. El-Bennich, G. Krein, L. Chang, C. D. Roberts, and D. J. Wilson, Phys. Rev. D **85**, 031502 (2012).

[50] K. U. Can, G. Erkol, M. Oka, A. Ozpineci, and T. T. Takahashi, Phys. Lett. B **719**, 103 (2013).

[51] L. Roca, E. Oset, and J. Singh, Phys. Rev. D **72**, 014002 (2005).

[52] D. Gamermann, J. Nieves, E. Oset, and E. Ruiz Arriola, Phys. Rev. D **81**, 014029 (2010).

[53] E. Oset and A. Ramos, Eur. Phys. J. A **44**, 445 (2010).

[54] E. J. Garzon and E. Oset, Eur. Phys. J. A **48**, 5 (2012).

[55] K. P. Khemchandani, A. Martinez Torres, H. Kaneko, H. Nagahiro, and A. Hosaka, Phys. Rev. D **84**, 094018 (2011).

[56] K. P. Khemchandani, H. Kaneko, H. Nagahiro, and A. Hosaka, Phys. Rev. D **83**, 114041 (2011).

[57] S. Sarkar, B.-X. Sun, E. Oset, and M. J. Vicente Vacas, Eur. Phys. J. A **44**, 431 (2010).

[58] M. B. Wise, Phys. Rev. D **45**, R2188 (1992).

[59] F. Mandl and G. Shaw, Quantum Field Theory (Wiley-Interscience, New York, 1984).

[60] L. Roca and E. Oset, Phys. Rev. D **82**, 054013 (2010).

[61] M. Bayar, J. Yamagata-Sekihara, and E. Oset, Phys. Rev. C **84**, 015209 (2011).

[62] J. M. Flynn, P. Fritzsch, T. Kawanai, C. Lehner, C. T. Sachrajda, B. Samways, R. S. Van de Water, and O. Witzel, arXiv:1311.2251.

[63] B. Borasoy, Phys. Rev. D **59**, 054021 (1999).

[64] R. C. Carrasco and E. Oset, Nucl. Phys. **A536**, 445 (1992).

[65] R. Machleidt, K. Holinde, and C. Elster, Phys. Rep. **149**, 1 (1987).

[66] E. Oset and M. J. Vicente-Vacas, Nucl. Phys. **A446**, 584 (1985).

[67] E. Oset, H. Toki, and W. Weise, Phys. Rep. **83**, 281 (1982).